IEEE Access
Multidisciplinary | Rapid Review | Open Access Journal

Received July 10, 2020, accepted July 24, 2020, date of publication August 3, 2020, date of current version August 17, 2020.

Digital Object Identifier 10.1109/ACCESS.2020.3013678

3D Printed OAM Reflectarray Using Half-Wavelength Rectangular Dielectric Element

BIN LI[1], (Member, IEEE), PENG FEI JING[2], LI QING SUN[1], KWOK WA LEUNG[3,4], (Fellow, IEEE), AND XIN LV[1]

[1]Beijing Key Laboratory of Millimeter Wave and Terahertz Technology, Beijing Institute of Technology, Beijing 100081, China
[2]Beijing Institute of Radio Measurement, Beijing 100854, China
[3]State Key Laboratory of Terahertz and Millimeter Waves and Department of Electrical Engineering, City University of Hong Kong, Kowloon, Hong Kong
[4]Shenzhen Key Laboratory of Millimeter Wave and Wideband Wireless Communications, CityU Shenzhen Research Institute, Shenzhen 518057, China

Corresponding author: Bin Li (eelibin@bit.edu.cn)

This work was supported in part by the National Natural Science Foundation of China under Grant 61771055, in part by the Basic Research Foundation of Beijing Institute of Technology under Grant 20170542009, and in part by the Research Grants Council of Hong Kong under Grant CityU 11217018.

ABSTRACT A 3D printed dielectric reflectarray is studied to generate orbital angular momentum (OAM) beam. The array element consists of a half-wavelength rectangular dielectric block and a metallic ground. It is found that the loss tangent and permittivity of the rectangular dielectric element independently affect the reflection magnitude and reflection phase, respectively. Four OAM modes ($l = 1, 2, 3, 4$) are theoretically studied. A prototype of the mode $l = 1$ working at Ka band is fabricated and measured. The maximum gain in the radiation direction ($\theta = 4°$) is 20.4 dBi at 30 GHz. A wide OAM bandwidth of 21.7% for the mode weight coefficient larger than 60% is also obtained. The proposed antenna shows its potential applications in OAM communications.

INDEX TERMS Reflectarray, dielectric resonator, orbital angular momentum, 3D printing.

I. INTRODUCTION

Increasing attention has been paid to orbital angular momentum (OAM) in microwave over the past decade. Various OAM modes are orthogonal with no interferences between channels, which is capable of improving communication capacities. Research on the OAM beam generation has notable growth since Allen *et al.* [1] found that a light beam carries an OAM by a phase dependence of azimuthal angle and topological charge. After that, various techniques have been used to generate the OAM beams, such as spiral phase plate [2], travelling-wave antenna [3], spiral reflector [4], high-order mode dielectric resonator (DR) antenna [5], and reflective metasurface [6].

Reflectarray has the advantages of low profile, lightweight, and high efficiency. A lot of research on reflectarray has been widely carried out on broadband, circular polarization, beam scanning, and terahertz [7], [8], but analysis on the OAM reflectarray [9] is relatively limited. In 2016, a square patch-based dual-beam OAM reflectarray was proposed [10]. In 2017, a Ka-band OAM folded reflectarray with a multi-resonance dipole element was studied [11]. In 2018, Meng *et al.* [12] reported a cross dipole combined with other three groups of resonant L shaped structures to achieve both linearly- and circularly-polarized (CP) OAM beams by rotating the feed polarization. In 2019, a double-layered rhombus-shaped patch OAM CP reflectarray was reported, with a wide axial ratio (AR) bandwidth of 20% [13]. Zhang *et al.* [14] studied a square-patch reflective metasurface, as well as a phased array antenna, for OAM multiplexing. Recently, a multi-resonance element consisting of three types of patches (loop, cross-dipole, four square patches) was demonstrated for wideband OAM reflectarray, which achieved 42% OAM bandwidth [15] for the mode weight coefficient larger than 70%. Nevertheless, current reflectarray elements are mainly microstrip structures, which suffer from high surface-wave loss and need high-cost microfabrication techniques, particularly in millimeter-wave and THz bands.

Because of its excellent characteristics such as low cost, low conductor loss, and low Q factor, dielectric resonator

The associate editor coordinating the review of this manuscript and approving it for publication was Wei E. I. Sha.

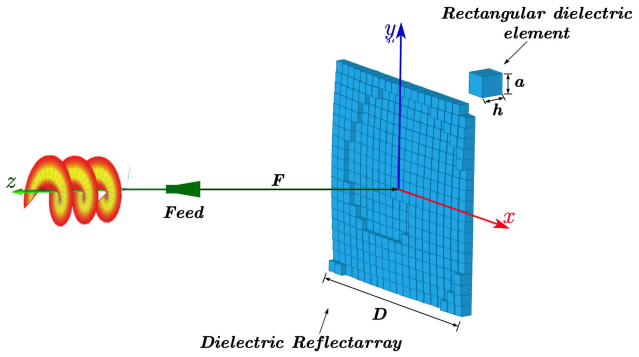

FIGURE 1. The geometry of the OAM reflectarray of the rectangular dielectric element.

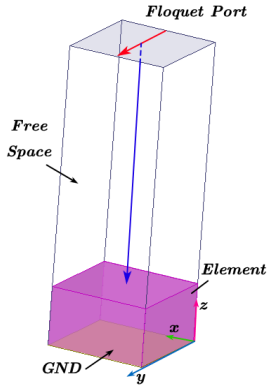

FIGURE 2. The HFSS model of the rectangular dielectric element.

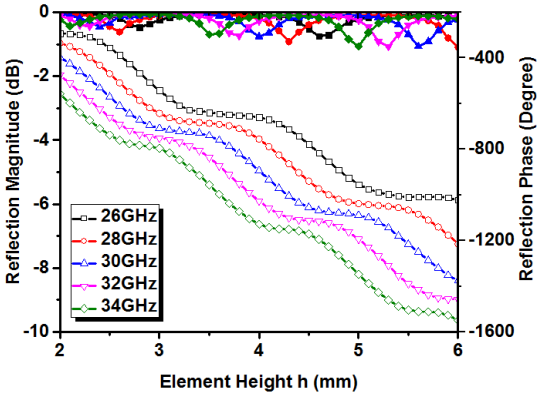

FIGURE 3. The reflection magnitude (left) and phase (right) versus element height for various frequencies.

antenna [16] has been extensively studied over the past three decades. In recent years, increasing attention has been paid to the dielectric reflectarrays at microwave band, such as dual-band [17], high frequency [18]–[20], wide-band [21], [22], and circular polarization [23]. In 2012, Alsath *et al.* [17] investigated a dual-band dielectric reflectarray operating at C/X band. In 2014, Nayeri *et al.* [18] studied a dielectric reflectarray working at 100 GHz. In 2017, by using a metamaterial-based impedance-matched element, He *et al.* [22] achieved a broad dielectric reflectarray of 18.1% gain bandwidth. Last year, we first proposed a CP dielectric reflectarray composed of the hemi-ellipsoidal element [23], which has a 3 dB AR bandwidth of 6.7%. Although dielectric reflectarrays of various characteristics have been studied, its OAM beam generation has not been well explored. Recently, an OAM dielectric reflectarray was proposed by perforating holes on the substrate [24], but only some limited simulation results were given.

In this article, an OAM reflectarray composed of the half-wavelength rectangular dielectric elements is studied. The effects of the dielectric loss tangent and permittivity on the reflection characteristics are investigated. It is found that the OAM beams of four modes ($l = 1, 2, 3, 4$) can be easily excited, and the OAM mode $l = 1$ is thoroughly studied. Results show that the maximum gain is 20.4 dBi at operating frequency $f_0 = 30$ GHz and radiation direction $\theta = 4°$. A relatively broad mode purity (MP) bandwidth of 21.7% can be easily achieved. A 3D printed prototype is fabricated and tested. Good agreement between simulated and measured results is obtained.

II. ELEMENT DESIGN AND ANALYSIS

Fig. 1 shows the structure of the proposed OAM dielectric reflectarray. The aperture diameter is D = 100 mm, and the focal distance is F = 300 mm. The pyramidal horn is used as the feed of the proposed reflectarray. The element simulation model is shown in Fig. 2. Each element consists of a rectangular dielectric block and a metallic ground. The dielectric constant of the material is $\varepsilon_r = 10$. The length and width of the dielectric block are the same (a = 5mm), which is approximately half a free-space wavelength of 30 GHz. Ansys HFSS is used for simulation, and the Floquet port excitation and master & slave boundaries are applied for analysis. Fig. 3 shows the reflective phase curves as a function of the element height at frequencies from 26GHz to 34GHz. It is found that a relatively significant phase shift of over 360° can be easily obtained through changing the element height h. By applying the linear fitting function to the phase-shifting curve, the quantitative relationship between the element height and reflection phase can be obtained, which can be used to determine the reflectarray dimensions. From the figure, it is also observed that the phase curves are almost parallel, showing a wideband characteristic of the proposed antenna.

Meanwhile, the dielectric material effects on the reflective magnitude and phase are also investigated. Firstly, the effect of loss tangent ($\tan\delta$) with the same permittivity $\varepsilon_r = 10$ is studied, as shown in Fig. 4. It is found that the reflection magnitude monotonously increases with the increase of loss tangent from 0.004 to 0.06, whereas the reflection phases are almost unchanged. In other words, the loss tangent mainly determines the antenna efficiency, not the reflection phase or the element dimension, which is to be expected. Secondly, the effect of the dielectric constant with the same

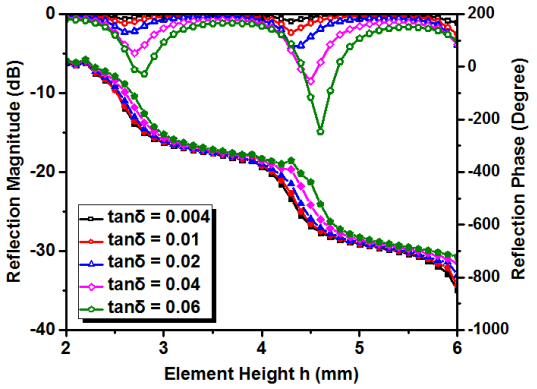

FIGURE 4. The reflection magnitude (left) and phase (right) versus element height for various loss tangent. The permittivity is $\varepsilon_r = 10$.

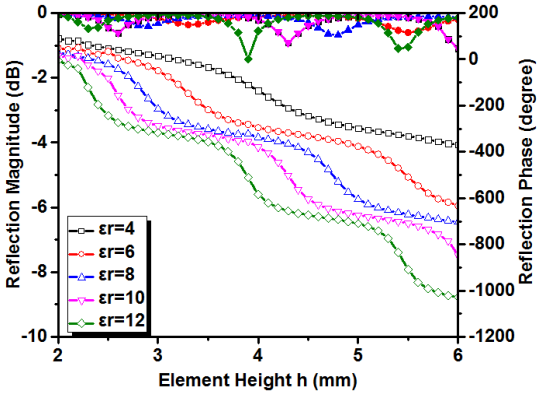

FIGURE 5. The reflection magnitude (left) and phase (right) versus element height for various dielectric constant. The loss tangent is tan $\delta = 0.004$.

TABLE 1. The loss tangent and permittivity effects on the reflection parameters.

tan δ (ε_r=10)	Reflection Magnitude (dB)	ε_r (tan δ=0.004)	Reflection Phase (degree)
0.004	-1	4	459
0.01	-2.5	6	682
0.02	-4.5	8	733
0.04	-8.5	10	863
0.06	-15	12	1022

loss tangent tan$\delta = 0.004$ is investigated. With reference to Fig. 5, the phase shift range also monotonously increases with the increase of dielectric constant from 4 to 12, while the magnitude curves keep stable. The results show that a high permittivity can facilitate the dielectric reflectarray design. The results are also displayed in Table 1 for clarity. It is worth mentioning that other element shapes such as cylindrical and hemispherical dielectric elements have also been studied. Similar results can be found, which is omitted here for brevity.

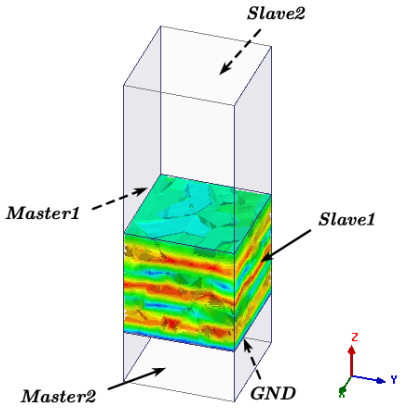

FIGURE 6. Electric field distribution of the dielectric element (a = h = $\lambda_0/2$) excited by a linearly polarized plane wave.

Fig. 6 shows the electric field distribution of the dielectric element excited by a plane wave, where the unit length, width, and height are equal to half wavelength in free space. The master and slave boundaries are used in the Floquet port to simulate the infinite periodic structure. The analysis process of this element is equivalent to that of an incident plane wave illuminating a fixed-thickness dielectric plate and returning to the free space after reflected by the metal ground. In the process of electromagnetic wave propagation, there are two boundary conditions worthy of attention: one is the boundary between the dielectric block and metal ground, the other is the boundary between free space and high dielectric constant element. The former is easy to understand as the PEC boundary brings total reflection of electromagnetic waves. While the latter is mainly due to the discontinuity between two kinds of media with a drastic change of ε_r, which leads to multiple reflections of the electromagnetic wave within the dielectric plate, that is a standing wave along the propagation direction as shown in Fig. 6. Since the height of the element is the half free-space wavelength, which is about three times the half dielectric wavelength in the dielectric material with $\varepsilon_r = 10$, three standing wave peaks can be observed in this figure.

It is found that the periodic variations of the reflection magnitude and phase are caused by the standing wave distribution of the dielectric element, as shown in Fig. 6. From Fig. 3 to 5, the reflection magnitude and phase are correlated. The phase difference between the two lowest magnitude points is about 360 degrees, which indicates a variation period. This phenomenon can also be explained by the electric field distribution of the dielectric element in Fig. 6, that is, within a range of standing wave variation ($\lambda g/2$), the element phase shift covers about 360 degrees. Therefore, the higher the element height is, the more standing waves are contained, which leads to an increase of total phase-shift range.

III. DESIGN OF MILLIMETER-WAVE OAM DIELECTRIC REFLECTARRAY

The procedure to obtain the antenna geometry is demonstrated as follows. Firstly, the element simulation is carried

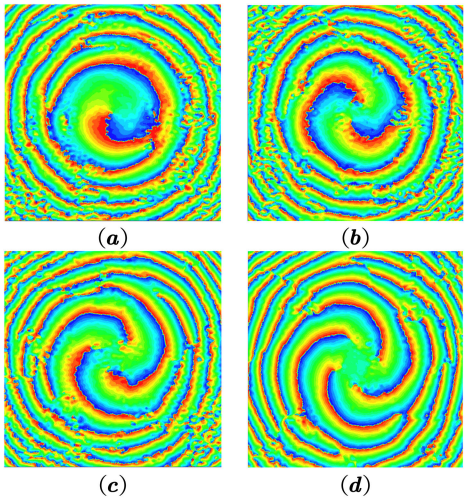

FIGURE 7. Wavefront phase distribution on the observational plane at z = 0.4m with four OAM modes at 30 GHz. (a) *l* = 1 (b) *l* = 2 (c) *l* = 3 (d) *l* = 4.

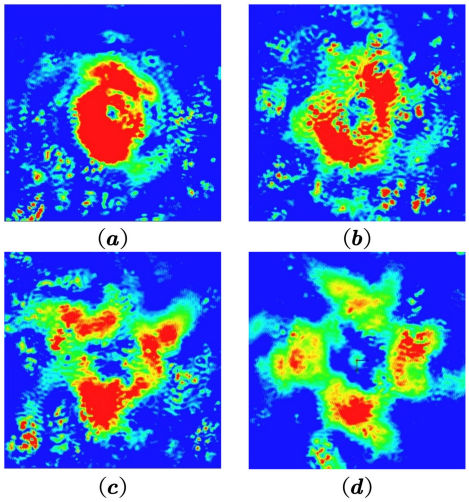

FIGURE 8. Wavefront magnitude distribution on the observational plane at z = 0.4m with four OAM modes at 30 GHz. (a) *l* = 1 (b) *l* = 2 (c) *l* = 3 (d) *l* = 4.

out to get the phase-shifting curve of the element. Secondly, the focal diameter ratio F/D and the feed position are determined by considering the feed beamwidth and aperture size. Thirdly, the compensated phase distribution is obtained based on the aperture phase synthesis. Finally, the physical parameters of the array can be obtained by using the element phase-shifting curve to convert the compensation phase into each unit geometry. By adjusting the reference phase of the array, the performance of the array beam can be optimized. Therefore, based on the element design, a rectangular OAM dielectric reflectarray is designed at the Ka band with the size 20×20, that is 100×100 mm^2, as shown in Fig. 1. The feeding horn antenna is placed in the boresight direction of the surface, which can minimize the shielding effect because of the zero magnitudes of the OAM beam. The height of the feeding horn is selected to be 0.3m to guarantee the -10 dB illuminated level at the edge of the surface, and the ratio between focal length and aperture diameter (F/D) is 3.0. The calculation process of the compensated surface phase distribution can be found in [6], which is omitted here for brevity.

Fig. 7 shows the wavefront of spiral phase distribution with four OAM modes ($l = 1, 2, 3, 4$) on the observational plane $z = 0.4$ m at 30 GHz. Due to the divergence of the OAM beam, we finally choose the observational plane with a size of 0.4×0.4 m^2 to view the magnitude and phase distribution of the electric field. Reasonable results of the four OAM modes are obtained. Fig. 8 shows the wavefront of the magnitude distribution of four OAM modes ($l = 1, 2, 3, 4$) on the observational plane. As the OAM mode number increases, the radius of the doughnut-shaped electrical field intensity gradually increases, which is related to the rise of the cone angle of the radiation pattern. The cone-shaped radiation pattern of mode $l = 1$ at 30 GHz is shown in Fig.9. An OAM beam with maximum

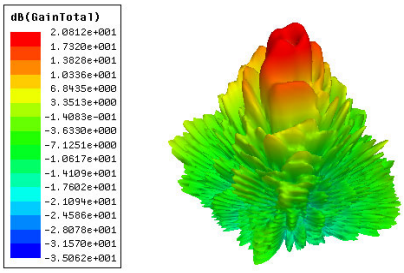

FIGURE 9. The simulated 3D radiation pattern for mode number *l* = 1 at 30GHz.

TABLE 2. Maximum antenna gain versus frequency in the vicinity of radiation direction $\theta = 4°$.

Frequency (GHz)	Gain (dBi)
28	18.2
29	20.2
30	20.4
31	20.6
32	20.3

radiation direction at $\theta = 4°$ is obtained, where the gain is 20.4 dBi.

Table 2 shows the maximum gain in the vicinity of radiation direction ($\theta = 4°$) versus frequency. The energy of the OAM beam is distributed along a specific cone angle, and the gain values slightly change at different azimuthal angles. It can be seen from the table that the maximum gain remains stable over a wide frequency range.

A prototype of the proposed OAM dielectric reflectarray with $l = 1$ fabricated using 3D printing technology is shown in Fig. 10(a). The Preperm 3D ABS DK 10.0 filament is

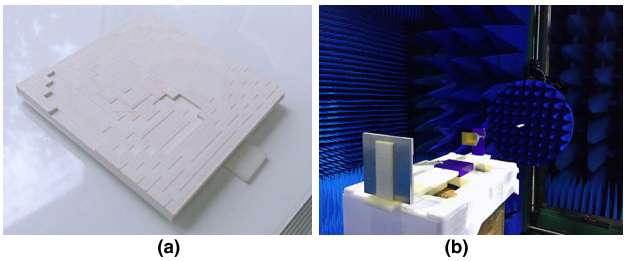

FIGURE 10. Prototype and measurement setup (a) Reflectarray prototype with $l = 1$ (b) OAM beam measurement setup using near-field scanning system.

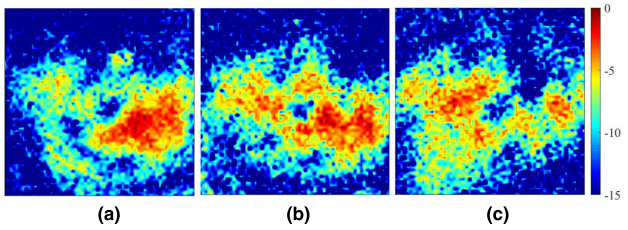

FIGURE 11. Measured electrical-field magnitude distribution on the near-field sampling plane at (a) 28 GHz (b) 30 GHz (c) 32 GHz.

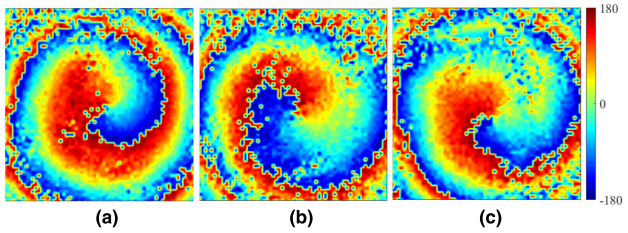

FIGURE 12. Measured electrical-field phase distribution on the near-field sampling plane at (a) 28 GHz (b) 30 GHz (c) 32 GHz.

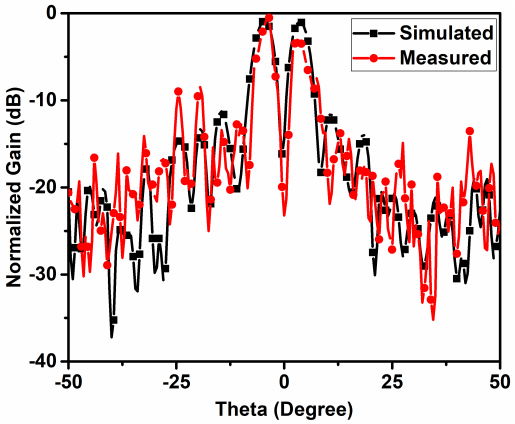

FIGURE 13. Simulated and measured xoz-plane radiation patterns at 30GHz.

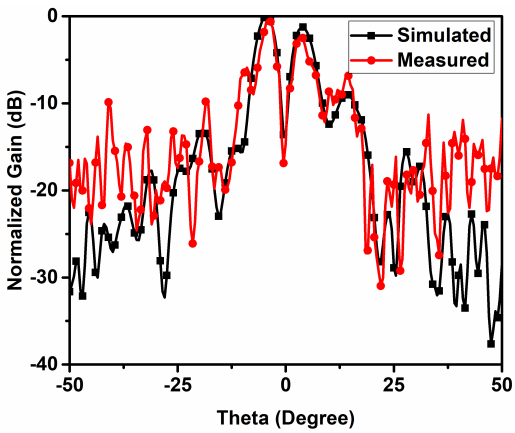

FIGURE 14. Simulated and measured yoz-plane radiation patterns at 30GHz.

selected with permittivity of 10 and dielectric loss tangent of 0.004. 3D printing procedure is accomplished with fused deposition modeling using Flashforge Creator Pro 3D Printer. A near-field planar scanning system of our lab, as shown in Fig. 10(b), was used to measure the proposed antenna. The vertical electric field E_v is measured using a standard Ka near-field waveguide probe, which is 0.6 m away from the reflectarray. The scanning step is 4.5 mm, and the near E-field value at each pixel can be obtained by scanning the probe along the x- and y-axis.

Fig.11 and 12 show the measured results of magnitude and phase distribution of Ev at 28 GHz, 30 GHz, and 32 GHz with relatively good consequences. As can be seen from the figure, the reflectarray achieves spiral phase distribution at different frequencies. Although the magnitude results are not ideal as compared to the simulated ones, it has little effect on OAM detection because the phase information is the main factor.

Fig.13 and Fig.14 show the simulated and measured xoz- and yoz-plane radiation patterns at 30 GHz with good agreement. A magnitude null point can be observed in the surface boresight direction, and the maximum radiation direction is found to be $\theta = 4°$.

To demonstrate the mode purity of the desired OAM mode ($l = 1$), Fourier transforms applies on the measured electric field results [25]. We consider the electric field $E_1(r, \varphi, z)$ with a defined OAM mode expansion, as shown in formula (1).

$$E_1(r, \varphi, z) = \frac{1}{\sqrt{2\pi}} \sum_{l=-\infty}^{\infty} a_l(r, z) \exp(jl\varphi) \tag{1}$$

In order to decompose different OAM modes of the field distribution, the components of the given OAM harmonic $\exp(jl\varphi)$ are calculated in (2)

$$a_l(r, z) = \frac{1}{\sqrt{2\pi}} \int_0^{2\pi} E_1(r, \varphi, z) \exp(-jl\varphi) \tag{2}$$

The energy carried by the corresponding mode number l can be written as

$$W_l = 2\varepsilon_0 \int_0^{\infty} |a_l(r, z)|^2 r dr \tag{3}$$

By adding all the OAM mode energy, the total electrical field energy can be obtained. Finally, the mode weighting

TABLE 3. Comparison of the proposed OAM dielectric reflectarray with some existing OAM reflectarrays.

Year	Ref	Element Type	Element Structure	Frequency (GHz)	Aperture Size (λ_0)	Polarization	Gain (dBi)	OAM Bandwidth
2016	[10]	Microstrip	Square patch	6	10	LP	17.0	16.7%
2017	[11]	Microstrip	multi-resonance dipole	32	10.88	LP	21.5	N/A
2019	[13]	Microstrip	Rhombus shaped patch	10	10.5	CP	19.9	N/A
2019	[15]	Microstrip	multi-resonance patch	6	10	LP	18.9	42%
2020	This work	Dielectric	Rectangular, $\lambda/2$	30	10	LP	20.4	21.7%

N/A: not available

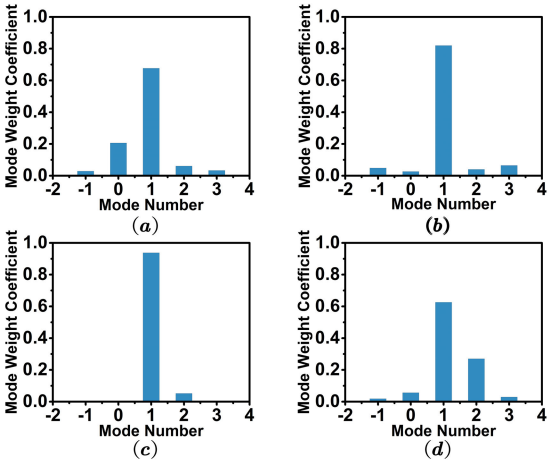

FIGURE 15. The measured OAM spectrum weight at (a) 26.5 GHz (b) 28 GHz (c) 30 GHz and (d) 32.5 GHz.

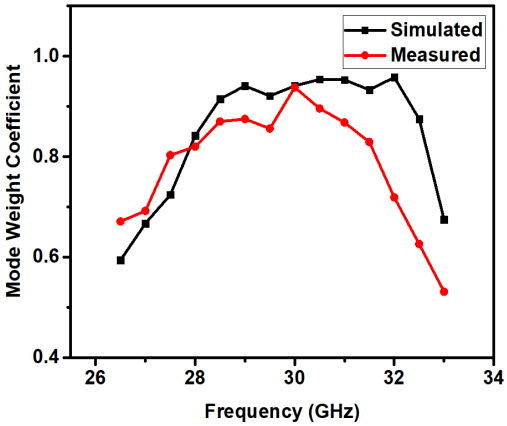

FIGURE 16. The simulated and measured OAM $l = 1$ mode weight coefficient versus frequency.

coefficient, that is ratio of mode energy to total energy, can be written as

$$M_l = \frac{W_l}{\sum_{q=-\infty}^{\infty} W_q} \tag{4}$$

Fig. 15 shows the vortex spectrum expansion results at different frequencies. From the figure, it can be observed that the mode weight coefficients of dominant mode ($l = 1$) reach 67.1%, 82%, 93.8%, and 62.6% at 26.5 GHz, 28 GHz, 30 GHz, and 32.5 GHz, respectively. By further analyzing the simulated and measured OAM mode purities versus frequency in Fig. 16, it can be easily observed that the simulated and measured bandwidths are 21.7% and 20.5%, respectively, for mode weight coefficient larger than 60%. Reasonable agreement between simulation and measurement can be obtained.

Table 3 compares the proposed dielectric OAM reflectarray with some existing microstrip OAM reflectarrays. It is found that the OAM bandwidth of the proposed dielectric reflectarray is higher than that of the microstrip reflectarray of the square patch element [10]. The gain is also higher than that of the multi-resonance reflectarray [15], but with less OAM bandwidth, which can be further improved using a complex dielectric element.

The reflectarray using a quarter-wavelength rectangular dielectric element is also studied. It is found that the results of the quarter-wavelength element reflectarray are almost the same as that of the half-wavelength counterpart, which indicates the element size has little effect on the OAM bandwidth performance. This is important because we can choose a relatively large element size to minimize the fabrication difficulty, which is especially useful for high- frequency applications.

IV. CONCLUSION

A Ka-band OAM dielectric reflectarray has been thoroughly investigated. It has been found that low dielectric loss and high dielectric constant will facilitate the design of dielectric reflectarray. A 20 × 20 elements 3D printed OAM dielectric reflectarray with a mode number of $l = 1$ has been fabricated and measured. A maximum gain of 20.4 dBi at 30 GHz and a relatively wide mode purity bandwidth of 21.7% have been obtained. Simulation results have been verified by measurement results with reasonable agreement.

These features make the proposed OAM dielectric reflectarray potentially useful in the next-generation communication system.

REFERENCES

[1] L. Allen, M. W. Beijersbergen, R. J. C. Spreeuw, and J. P. Woerdman, "Optical angular momentum of light and the transformation of Laguerre–Gauss laser modes," *Phys. Rev. A, Gen. Phys.*, vol. 45, no. 11, pp. 8185–8189, Jun. 1992.
[2] X. Hui, S. Zheng, Y. Hu, C. Xu, X. Jin, H. Chi, and X. Zhang, "Ultralow reflectivity spiral phase plate for generation of millimeter-wave OAM beam," *IEEE Antennas Wireless Propag. Lett.*, vol. 14, pp. 966–969, 2015.
[3] Z. Zhang, S. Zheng, X. Jin, H. Chi, and X. Zhang, "Generation of plane spiral OAM waves using traveling-wave circular slot antenna," *IEEE Antennas Wireless Propag. Lett.*, vol. 16, pp. 8–11, 2017.
[4] E. Mari, F. Spinello, M. Oldoni, R. A. Ravanelli, F. Romanato, and G. Parisi, "Near-field experimental verification of separation of OAM channels," *IEEE Antennas Wireless Propag. Lett.*, vol. 14, pp. 556–558, 2015.
[5] J. Ren and K. W. Leung, "Generation of microwave orbital angular momentum states using hemispherical dielectric resonator antenna," *Appl. Phys. Lett.*, vol. 112, no. 13, Mar. 2018, Art. no. 131103.
[6] S. Yu, L. Li, G. Shi, C. Zhu, X. Zhou, and Y. Shi, "Design, fabrication, and measurement of reflective metasurface for orbital angular momentum vortex wave in radio frequency domain," *Appl. Phys. Lett.*, vol. 108, no. 12, Mar. 2016, Art. no. 121903.
[7] P. Nayeri, F. Yang, and A. Z. Elsherbeni, *Reflectarray Antennas: Theory, Designs, and Applications*. Hoboken, NJ, USA: Wiley, 2018.
[8] S.-W. Qu, H. Yi, B. J. Chen, K. B. Ng, and C. H. Chan, "Terahertz reflecting and transmitting metasurfaces," *Proc. IEEE*, vol. 105, no. 6, pp. 1166–1184, Jun. 2017.
[9] M. Veysi, C. Guclu, F. Capolino, and Y. Rahmat-Samii, "Revisiting orbital angular momentum beams: Fundamentals, reflectarray generation, and novel antenna applications," *IEEE Antennas Propag. Mag.*, vol. 60, no. 2, pp. 68–81, Apr. 2018.
[10] S. Yu, L. Li, G. Shi, C. Zhu, and Y. Shi, "Generating multiple orbital angular momentum vortex beams using a metasurface in radio frequency domain," *Appl. Phys. Lett.*, vol. 108, no. 24, Jun. 2016, Art. no. 241901.
[11] X. Y. Lei and Y. J. Cheng, "High-efficiency and high-polarization separation reflectarray element for OAM-folded antenna application," *IEEE Antennas Wireless Propag. Lett.*, vol. 16, pp. 1357–1360, 2017.
[12] X.-S. Meng, J.-J. Wu, Z.-S. Wu, T. Qu, and L. Yang, "Design of multiple-polarization reflectarray for orbital angular momentum wave in radio frequency," *IEEE Antennas Wireless Propag. Lett.*, vol. 17, no. 12, pp. 2269–2273, Dec. 2018.
[13] G.-T. Chen, Y.-C. Jiao, and G. Zhao, "A reflectarray for generating wideband circularly polarized orbital angular momentum vortex wave," *IEEE Antennas Wireless Propag. Lett.*, vol. 18, no. 1, pp. 182–186, Jan. 2019.
[14] D. Zhang, X. Cao, J. Gao, H. Yang, W. Li, T. Li, and J. Tian, "A shared aperture 1 bit metasurface for orbital angular momentum multiplexing," *IEEE Antennas Wireless Propag. Lett.*, vol. 18, no. 4, pp. 566–570, Apr. 2019.
[15] Z. Akram, X. Li, Z. Qi, A. Aziz, L. Yu, H. Zhu, X. Jiang, and X. M. Li, "Wideband vortex beam reflectarray design using quarter-wavelength element," *IEEE Antennas Wireless Propag. Lett.*, vol. 18, no. 7, pp. 432–436, Jul. 2019.
[16] K. W. Leung, E. H. Lim, and X. S. Fang, "Dielectric resonator antennas: From the basic to the aesthetic," *Proc. IEEE*, vol. 100, no. 7, pp. 2181–2193, Jul. 2012.
[17] M. G. N. Alsath, M. Kanagasabai, and S. Arunkumar, "Dual-band dielectric resonator reflectarray for C/X-bands," *IEEE Antennas Wireless Propag. Lett.*, vol. 11, pp. 1253–1256, 2012.
[18] P. Nayeri, M. Liang, R. A. Sabory-Garcia, M. Tuo, F. Yang, M. Gehm, H. Xin, and A. Z. Elsherbeni, "3D printed dielectric reflectarrays: Low-cost high-gain antennas at sub-millimeter waves," *IEEE Trans. Antennas Propag.*, vol. 62, no. 4, pp. 2000–2008, Apr. 2014.
[19] M. D. Wu, B. Li, Y. Zhou, D. L. Guo, Y. Liu, F. Wei, and X. Lv, "Design and measurement of a 220 GHz wideband 3-D printed dielectric reflectarray," *IEEE Antennas Wireless Propag. Lett.*, vol. 17, no. 11, pp. 2094–2098, Nov. 2018.
[20] M. K. T. Al-Nuaimi and W. Hong, "Discrete dielectric reflectarray and lens for E-band with different feed," *IEEE Antennas Wireless Propag. Lett.*, vol. 13, pp. 947–950, 2014.
[21] Y.-X. Sun and K. W. Leung, "Millimeter-wave substrate-based dielectric reflectarray," *IEEE Antennas Wireless Propag. Lett.*, vol. 17, no. 12, pp. 2329–2333, Dec. 2018.
[22] Y. He, Z. Gao, D. Jia, W. Zhang, B. Du, and Z. N. Chen, "Dielectric metamaterial-based impedance-matched elements for broadband reflectarray," *IEEE Trans. Antennas Propag.*, vol. 65, no. 12, pp. 7019–7028, Dec. 2017.
[23] X. Zhao, F. Wei, B. Li, and X. Shi, "Design of circularly polarized dielectric resonator reflectarray antenna," in *Proc. Asia–Pacific Microw. Conf. (APMC)*, Kyoto, Japan, Nov. 2018, pp. 1552–1554.
[24] X. Bai, X. Liang, C. He, Y. Li, L. Liu, J. Chen, M. Liu, J. Geng, and R. Jin, "Perforated dielectric antenna reflectarray for OAM generation," in *Proc. IEEE Int. Symp. Antennas Propag., USNC/URSI Nat. Radio Sci. Meeting*, Vancouver, BC, Canada, Jul. 2015, pp. 2159–2160.
[25] L. Torner, J. P. Torres, and S. Carrasco, "Digital spiral imaging," *Opt. Express*, vol. 13, no. 3, pp. 873–881, 2005.

BIN LI (Member, IEEE) was born in Tianjin, China. He received the B.Eng. degree from Xidian University, Xi'an, China, in 2001, and the Ph.D. degree from the City University of Hong Kong, in 2007, all in electronic engineering. In 2007, he joined the School of Information and Electronics, Beijing Institute of Technology (BIT), Beijing, China, where he is currently an Associate Professor. In 2009, he was a Research Fellow with the State Key Laboratory of Millimeter Waves, City University of Hong Kong. His research interests include antenna design, computational electromagnetics, metamaterial, and millimeter-wave/THz.

PENG FEI JING was born in Shanxi, China. He received the B.S. degree in electromagnetic field and wireless technology from Xidian University, Xi'an, China, in 2017, and the M.S. degree in electromagnetic field and microwave technology from the Beijing Institute of Technology, Beijing, China, in 2020. He is currently pursuing with the Beijing Institute of Radio Measurement, Beijing. His current research interests include reflectarray antennas, RF circuits, and metasurface.

LI QING SUN was born in Tianjin, China, in 1996. She received the B.E. degree from Xidian University, Xi'an, China, in 2018. She is currently pursuing the M.E. degree with the Beijing Institute of Technology, Beijing, China. Her current research interests include microstrip/dielectric reflectarrays and metasurface.

KWOK WA LEUNG (Fellow, IEEE) was born in Hong Kong. He received the B.Sc. degree in electronics and the Ph.D. degree in electronics engineering from The Chinese University of Hong Kong, Hong Kong, in 1990 and 1993, respectively. In 1994, he joined the Department of Electronic Engineering, City University of Hong Kong (CityU), where he is currently the Chair Professor. From January 2006 to June 2006, he was a Visiting Professor with the Department of Electrical Engineering, The Pennsylvania State University, State College, PA, USA. His research interests include antenna designs and EM theory. He is currently a member of the AP-S Distinguished Lecturer Program Committee. He received the International Union of Radio Science (USRI) Young Scientists Awards in Japan and Russia, in 1993 and 1995. He also received the CityU Research Excellence Award, in 2013, and Departmental Outstanding Teacher Awards, in 2005, 2010, and 2011. He also received the prestigious First Class Award (Natural Science) in the 2016 Higher Education Outstanding Scientific Research Output Awards (Science and Technology) of the Ministry of Education, China. His students received the First Prize of the PIERS 2019 Best Student Paper Award (Subcommittee 4), the 2015 iWEM Student Best Paper Award, the 2015 IEEE AP-S Eugene F. Knott Memorial Pre-Doctoral Research Award, and the 2014 IEEE MTT-S Undergraduate/Pre-Graduate Scholarship. He was the Chair of the IEEE AP/MTT Hong Kong Joint Chapter, in 2006 and 2007. He was the Technical Program Chair of the 2008 Asia-Pacific Microwave Conference, Hong Kong; and the Technical Program Co-Chair of the 2006 IEEE TENCON, Hong Kong. He was a Guest Editor of the *IET Microwaves, Antennas and Propagation*. He served as an Associate Editor for the IEEE ANTENNAS AND WIRELESS PROPAGATION LETTERS. He was also an Associate Editor of the IEEE TRANSACTIONS ON ANTENNAS AND PROPAGATION and received Transactions Commendation Certificates twice, in 2009 and 2010, for his exceptional performance. He was the Editor-in-Chief of the Transactions, from 2013 to 2016. He was a Distinguished Lecturer of the IEEE Antennas and Propagation Society.

XIN LV received the B.S., M.S., and Ph.D. degrees in electronic engineering from the Beijing Institute of Technology (BIT), Beijing, China, in 1982, 1988, and 1993, respectively. Since 1982, he has been with BIT as a Lecturer, an Associate Professor, and a Professor. He also serves BIT as the Director of the Beijing Key Laboratory of Millimeter wave and Terahertz Technology. His research interests include millimeter wave and terahertz circuits, antennas, and systems.